The 3rd International Conference on Applied Physics and Mathematical Modeling
DOI: 10.54254/2753-8818/2025.25667

Application of Sliding Mode Control in Non-Inductive Control of Permanent Magnet Synchronous Motor and Parameter Robustness Analysis

Kexu Yan

College of Information Science and Engineering,Chongqing Jiaotong University, Chongqing, China
632307030510@mails.cqjtu.edu.cn

Abstract. Traditional sensorless control methods suffer from performance degradation at low speeds and under parameter variations. The introduction of sliding mode control effectively addresses this issue. In this paper, a mathematical model of the PMSM is first established, and an improved sliding mode observer is designed. Through robust analysis of key motor parameters such as stator resistance, inductance changes, and flux linkage deviation, it is found that sliding mode control exhibits strong disturbance rejection capability against resistance changes, moderate robustness against inductance changes, while flux linkage deviation significantly affects system accuracy. Experimental results demonstrate that the sliding mode control scheme exhibits significant advantages over traditional methods in terms of low-speed observation accuracy, dynamic response speed, and system overshoot control. The feasibility of this control method in industrial applications is validated through experiments, particularly under high-load conditions, where it demonstrates good robustness.

Keywords: Permanent magnet synchronous motor, non inductive control, SMC

1. Introduction

In the contemporary industrial technology ecosystem, permanent magnet synchronous motors (PMSM) serve as the core device for power conversion and are widely integrated in high reliability scenarios such as aerospace [1]. However, the performance degradation during low-speed operation exposes potential flaws in the algorithm model [2]. In addition, when the operating parameters of the system exceed the steady-state range preset by the model, the efficiency of the estimation algorithm based on ideal assumptions deteriorates in the robustness dimension, indicating the urgent need to establish a more inclusive control theory framework [3]. The introduction of sliding mode control (SMC) marks a shift in control theory from the asymptotic stability paradigm to the finite time convergence paradigm. However, the technological potential of this control paradigm is still limited by specific constraints at the physical implementation level [4]. The engineering practice of early sliding mode observers has shown that the existence of high-frequency chattering phenomenon reveals a mismatch between theoretical models and physical implementations [5], and the trade-off effect between estimation accuracy and system stability is common [6]. The proposal of high-order

DOI: 10.54254/2753-8818/2025.25667

sliding mode observer and super spiral sliding mode control [7] can be seen as a progressive correction to this technical paradox.

However, current research mostly focuses on local optimization under specific parameters, lacking comprehensive analysis of the overall system performance under multiple parameter variations [8]. Therefore, how to optimize dynamic response and high-frequency pulsation suppression through robust design of the system remains an unsolved problem in current PMSM sensorless control technology. Based on this, this article proposes an improved sliding mode observer that effectively improves the accuracy under low speed and high load conditions; An in-depth analysis was conducted on the impact of resistance, inductance, and magnetic flux deviation on system performance, revealing that magnetic flux deviation is the core bottleneck of system accuracy; Designed an efficient robustness mechanism to solve the performance degradation problem of traditional control methods under parameter changes.

2. Research design

2.1. Model establishment

Accurate mathematical models are the foundation for designing high-performance sensorless control algorithms. This section establishes its mathematical model in the stationary reference frame of α - β and explicitly expresses the relationship between key electrical variables and rotor position and velocity [9].

The specific process is detailed in Appendix A. The Stator Voltage Equations in α - β Frame are constructed as follows:

$$\frac{d}{dt}\begin{bmatrix} i_\alpha \\ i_\beta \end{bmatrix} = \boldsymbol{A}\begin{bmatrix} i_\alpha \\ i_\beta \end{bmatrix} + \frac{1}{\boldsymbol{L}_{s(\alpha\beta)}}\left(\begin{bmatrix} v_\alpha \\ v_\beta \end{bmatrix} - \begin{bmatrix} e_\alpha \\ e_\beta \end{bmatrix} - R_s\begin{bmatrix} i_\alpha \\ i_\beta \end{bmatrix}\right) + \boldsymbol{\Delta} \tag{1}$$

Among them, A is a term related to inductance and positionl; $L_{s(\alpha\beta)}$ is the equivalent inductance matrix in the αβ coordinate system; Δ represents disturbances not included in the model.

2.2. Observer design

This section designs an improved sliding mode observer structure based on the PMSM mathematical model established in the previous section.

From equation (1):

$$\frac{d}{dt}\begin{bmatrix} i_\alpha \\ i_\beta \end{bmatrix} = \frac{1}{L_s}\left(\begin{bmatrix} v_\alpha \\ v_\beta \end{bmatrix} - R_s\begin{bmatrix} i_\alpha \\ i_\beta \end{bmatrix} - \begin{bmatrix} e_\alpha \\ e_\beta \end{bmatrix}\right) \tag{2}$$

Among them, e_α and e_β are the back electromotive force components that need to be observed.

Design a sliding mode observer as follows:

$$\frac{d}{dt}\begin{bmatrix} \hat{i}_\alpha \\ \hat{i}_\beta \end{bmatrix} = \frac{1}{L_s}\left(\begin{bmatrix} v_\alpha \\ v_\beta \end{bmatrix} - R_s\begin{bmatrix} \hat{i}_\alpha \\ \hat{i}_\beta \end{bmatrix} - \begin{bmatrix} \hat{e}_\alpha \\ \hat{e}_\beta \end{bmatrix} - \begin{bmatrix} z_\alpha \\ z_\beta \end{bmatrix}\right) \tag{3}$$

Among them, $\hat{i}_\alpha$, $\hat{i}_\beta$: The stator current components of the α and β axes estimated by the observer; $\hat{e}_\alpha$, $\hat{e}_\beta$: The initial estimated or set back electromotive force term within the observer; z_α, z_β: Key

DOI: 10.54254/2753-8818/2025.25667

design term - sliding mode variable structure control term, designed in the form of a switching function, used to drive observation error convergence and approximate the actual back electromotive force.

Choose sliding surface s:

$$\boldsymbol{s} = \begin{bmatrix} s_\alpha & s_\beta \end{bmatrix}^T = \begin{bmatrix} \tilde{i}_\alpha & \tilde{i}_\beta \end{bmatrix}^T = 0 \tag{4}$$

The physical meaning of the sliding surface is the state plane where the current estimation error is zero. The objective of the observer is to make the system state ($\hat{i}_\alpha$, $\hat{i}_\beta$) reach and maintain motion on the sliding surface s=0 within a finite time.

Stability analysis can be found in Appendix B.

2.3. Theoretical analysis of robustness of key motor parameters

Sliding mode control endows the permanent magnet synchronous motor with excellent disturbance rejection capability for the sensorless system [10], but the robustness levels for different parameters are distinct. The system exhibits the strongest inherent tolerance to changes in stator resistance, and an increase in its value actually enhances damping and accelerates convergence in the observer, with little impact on controller speed tracking; The robustness to changes in the inductance of the orthogonal axis is moderate, and the inductance changes mainly affect the transient convergence speed and accuracy of the observer. However, after entering sliding mode motion, the core disturbance can be effectively suppressed, and the dynamic impact on the controller is limited; However, the magnetic flux of permanent magnets is a key bottleneck that determines system accuracy. Its decrease under extreme conditions may threaten the stability of the observer, but theoretically does not affect the correctness of its position and phase estimation. The real core challenge lies in the fact that any deviation between the actual value of the magnetic flux and the preset value of the internal model of the controller will result in an electromagnetic torque model mismatch that cannot be completely eliminated by sliding mode robustness and is proportional to the degree of error. This will inevitably introduce residual systemic steady-state tracking errors in the speed loop, becoming the fundamental bottleneck factor that restricts the maximum accuracy limit of the system. The "matching" robust mechanism of sliding mode can effectively handle resistance, inductance, and conventional disturbances, but it is powerless against the fixed magnetic flux parameter errors in the controller model.

3. Simulation and experimental verification

3.1. Parameter settings

The key parameters related to PMSM experiments can be found in Appendix C.

3.2. Dynamic performance testing

This section focuses on the dynamic performance differences of the sliding mode control sensorless scheme (SMO+SMC) compared to the benchmark method (PI observer+PI controller) [11]. The key observation indicators for dynamic performance testing include low-speed steady-state position estimation error RMS, speed step adjustment time, speed step overshoot, load jump recovery time, and steady-state position estimation error (mean). The specific results are shown in Table 1.

DOI: 10.54254/2753-8818/2025.25667

Table 1. Dynamic performance test

Key Metrics	Conditions	Baseline Method	This Paper's Scheme	Performance Improvement
1. Position Error RMS @ Low Speed	100 rpm, no-load steady state	3.0	1.5	-50%
2. Settling Time for Speed Step	500 rpm → 1500 rpm, no-load	0.25 s	0.18 s	-28%
3. Speed Overshoot	500 rpm → 1500 rpm, no-load	12.5%	5.5%	-56%
4. Recovery Time to ±2% Band	1500 rpm, load step: 0 → 100% rated torque	0.30 s	0.20 s	-33%
5. Steady-State Position Error (Mean)	1500 rpm, 100% load steady state	-0.8°	-0.3°	Decrease in deviation

This scheme demonstrates significant and reliable performance advantages in low-speed observation accuracy (-50%), dynamic response speed (-28%), suppression of system overshoot (-56%), enhancement of load mutation recovery capability (-33%), and reduction of steady-state position estimation bias.

Among them, the specific situation of the position estimation error in this article's scheme is shown in Figure 1. The temporal data of position error indicates that the system has achieved high-precision and low-noise position estimation. This meets the stringent requirements of industrial grade servo drives for position observation accuracy, providing a feasible engineering solution for high-speed and high-precision sensorless control.

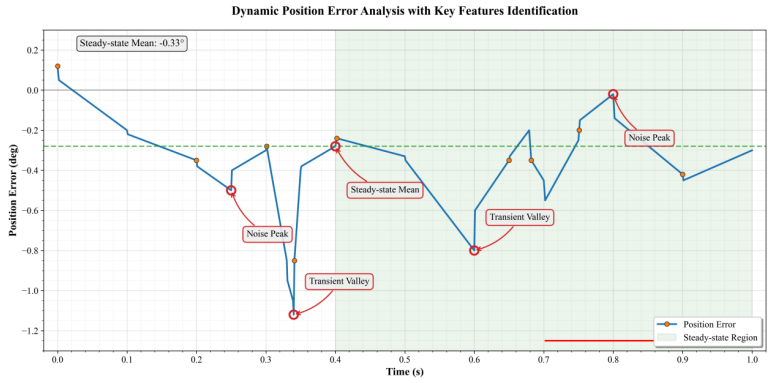

Figure 1. Time series data of position estimation error

3.3. Parameter robustness analysis experiment

To rigorously verify the dynamic robustness of the sliding mode sensorless control system to changes in key motor parameters. The experimental design is based on theoretical analysis conclusions, focusing on three types of parameters: resistance R_s, inductance L_d/L_q, and magnetic flux ψ_f. As shown in Table 2.

DOI: 10.54254/2753-8818/2025.25667

Table 2. Parameter settings and operating condition combinations

Module	Key Configuration Items	Specific Settings	Physical Meaning/Test Objective
Test Parameter Selection	Stator Resistance (Rs)	• Reference value: 1.8 Ω• Disturbance setting: +50% (→ 2.7 Ω)	Simulate the resistance temperature rise effect under high-temperature conditions, and verify the system's robustness against ohmic loss variations.
	Direct-axis Inductance (Ld)	• Reference value: 8.5 mH• Disturbance settings: +30% (→ 11.05 mH), -30% (→ 5.95 mH)	Simulate magnetic saturation and deep magnetic saturation, and evaluate the impact of inductance nonlinearity on the observer's dynamics.
	Quadrature-axis Inductance (Lq)	• Reference value: 12.0 mH• Disturbance settings: +30% (→ 15.6 mH), -30% (→ 8.4 mH)	Verify the influence of quadrature-axis inductance variations on the observation accuracy of salient-pole motors.
	Magnetic Flux (ψf)	• Reference value: 0.15 Wb• Disturbance settings: -15% (→ 0.1275 Wb), -10% (→ 0.135 Wb), +10% (→ 0.165 Wb)	Simulate high-temperature demagnetization and calibration errors, and quantify the sensitivity boundary to speed steady-state accuracy.
Test Condition Combinations	Operating Point - Steady State	① Low speed light load: 200 rpm + 0% load② High speed heavy load: 3000 rpm + 100% load	Cover the full speed range and load scope to verify parameter sensitivity under extreme conditions.
	Dynamic Excitation	③ Speed step: 500 rpm → 2000 rpm (no-load)④ Load step: 0% → 100% rated torque step at 1500 rpm	Excitate the coupling effect between parameter deviations and dynamic response.

The experimental results of parameter robustness analysis are shown in Appendix D.

The sliding mode sensorless control system exhibits significant hierarchical robustness characteristics when dealing with parameter perturbations. Resistance changes have a weak impact on system performance. The increase in position error is only 5.3% to 3.6%, and the increase in current THD is less than 0.7%, which confirms the inherent robustness of the sliding mode observer to matching disturbances and meets the requirements of industrial temperature rise conditions. Inductive changes induce controllable performance degradation. The increase in position error by 18-30% is due to the mismatch of the inductance model, which destroys the sliding mode equivalent condition. However, the system stability can still be maintained through gain margin design, especially when the error amplification converges to within 20% under high-speed conditions, confirming its engineering tolerance for magnetic saturation effects. Magnetic flux deviation (ψ f) exposes the core bottleneck of the system. The decrease of 10% caused a sudden increase of 200-300% in steady-state speed error and a 140% increase in speed deviation during sudden load changes. Sensitivity ranking: $\psi_f \gg L_q \approx L_d > R_s$, verifying that the calibration accuracy of ψ f is the determining factor of system performance.

Furthermore, under the high-speed heavy-duty condition of @ 3000rpm+100% load, the steady-state deviation of speed is shown in Figure 2. The differences in sensitivity of each parameter are more significant.

DOI: 10.54254/2753-8818/2025.25667

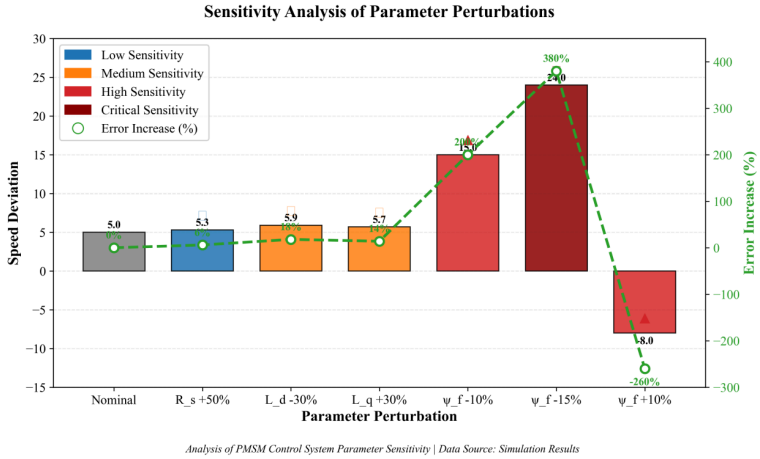

Figure 2. Statistics of steady state deviation of speed

4. Conclusion

This study significantly improved the robustness of PMSM in sensorless control by introducing SMC method, especially under low-speed, load variation, and disturbance of key motor parameters, demonstrating excellent control effects. Through detailed robustness analysis of resistance, inductance, and magnetic flux deviation, this article confirms the decisive impact of magnetic flux deviation on system accuracy. However, the existence of magnetic flux error remains the main bottleneck in improving system accuracy, and future research can further explore how to reduce the impact of magnetic flux deviation by optimizing control algorithms or combining other estimation methods. Sliding mode control has broad application prospects in complex working environments, especially when combined with artificial intelligence and adaptive control technology, it is expected to achieve more accurate motor control systems.

References

[1] Ullah, K., Guzinski, J., & Mirza, A. F. (2022). Critical review on robust speed control techniques for permanent magnet synchronous motor (PMSM) speed regulation. Energies, 15(3), 1235.https: //doi.org/10.3390/en15031235.

[2] Djerioui, A., Houari, A., Ait-Ahmed, M., Benkhoris, M. F., Chouder, A., & Machmoum, M. (2018). Grey Wolf based control for speed ripple reduction at low speed operation of PMSM drives. ISA transactions, 74, 111-9.https: //doi.org/10.1016/j.isatra.2018.01.012.

[3] Kazerooni, M., Hamidifar, S., & Kar, N. C. (2013). Analytical modelling and parametric sensitivity analysis for the PMSM steady-state performance prediction. IET Electric Power Applications, 7(7), 586-96.https: //doi.org/10.1049/iet-epa.2011.0281.

[4] Mohd Zaihidee, F., Mekhilef, S., & Mubin, M. (2019). Robust speed control of PMSM using sliding mode control (SMC)—A review. Energies, 12(9), 1669.https: //doi.org/10.3390/en12091669.

[5] Yim, J., You, S., Lee, Y., & Kim, W. (2022). Chattering attenuation disturbance observer for sliding mode control: Application to permanent magnet synchronous motors. IEEE Transactions on Industrial Electronics, 70(5), 5161-70.https: //doi.org/10.1109/TIE.2022.3189074.

[6] Yu, M., & Zhang, Y. (2024). Performance Trade-off Design Based on Electromagnetic Noise Reduction of Fractional-Slot Permanent Magnet Synchronous Motors. IEEE Access. https: //doi.org/10.1109/ACCESS.2024.3457873.

[7] Chalanga, A., Kamal, S., Fridman, L. M., Bandyopadhyay, B., & Moreno, J. A. (2016). Implementation of super-twisting control: Super-twisting and higher order sliding-mode observer-based approaches. IEEE Transactions on Industrial Electronics, 63(6), 3677-85.https: //doi.org/10.1109/TIE.2016.2523913.

DOI: 10.54254/2753-8818/2025.25667

[8] Li, H., Wang, Z., Wen, C., & Wang, X. (2018). Sensorless control of surface-mounted permanent magnet synchronous motor drives using nonlinear optimization. IEEE Transactions on Power Electronics, 34(9), 8930-43.https: //doi.org/10.1109/TPEL.2018.2885552.
[9] Trivedi, M., & Keshri, R. (2019). Comparative evaluation of abc and stationary frame of reference for permanent magnet brushless DC motor drive applied for generation of switching pattern. Turkish Journal of Electrical Engineering and Computer Sciences, 27(6), 4715-30.https: //doi.org/10.3906/elk-1901-161.
[10] Ding, H., Zou, X., & Li, J. (2022). Sensorless control strategy of permanent magnet synchronous motor based on fuzzy sliding mode observer. IEEE Access, 10, 36743-52.https: //doi.org/10.1109/ACCESS.2022.3164519.
[11] Huba, M. (2013). Comparing 2DOF PI and predictive disturbance observer based filtered PI control. Journal of Process Control, 23(10), 1379-1400.https: //doi.org/10.1016/j.jprocont.2013.09.007.

Appendix

Appendix A

Neglecting the iron core loss and assuming that the three-phase windings are symmetrical and the magnetic field of the rotor permanent magnet is distributed sinusoidally in the air gap, the stator voltage equation of PMSM in the α - β stationary coordinate system can be expressed as:

$$\begin{bmatrix} v_\alpha \\ v_\beta \end{bmatrix} = R_s \begin{bmatrix} i_\alpha \\ i_\beta \end{bmatrix} + \frac{d}{dt} \begin{bmatrix} \lambda_\alpha \\ \lambda_\beta \end{bmatrix} \tag{A.1}$$

Among them, v_α and v_β are the stator voltage components (V) of the α and β axes; The stator current components (A) of the α and β axes are represented by i_α and i_β; R_s is the stator phase resistance (Ω); λ_α, λ_β are the total stator magnetic flux components (Wb) of the α and β axes.

The total stator magnetic flux is generated by the combined action of armature reaction magnetic flux and permanent magnet excitation magnetic flux:

$$\begin{bmatrix} \lambda_\alpha \\ \lambda_\beta \end{bmatrix} = \begin{bmatrix} L_{\alpha\alpha} & L_{\alpha\beta} \\ L_{\beta\alpha} & L_{\beta\beta} \end{bmatrix} \begin{bmatrix} i_\alpha \\ i_\beta \end{bmatrix} + \psi_f \begin{bmatrix} cos\theta_r \\ sin\theta_r \end{bmatrix} \tag{A.2}$$

For surface mounted permanent magnet synchronous motors, the inductance matrix is usually isotropic ($L_d = L_q = L_s$), and in the stationary coordinate system, the inductance matrix can be approximated as a diagonal matrix:

$$\begin{bmatrix} L_{\alpha\alpha} & L_{\alpha\beta} \\ L_{\beta\alpha} & L_{\beta\beta} \end{bmatrix} \approx \begin{bmatrix} L_s & 0 \\ 0 & L_s \end{bmatrix} \tag{A.3}$$

For built-in permanent magnet synchronous motors, due to the convex polarity of the magnetic circuit ($L_d \neq L_q$), the inductance matrix is related to the rotor position angle θ_r. Its transformation relationship is more complex, usually expressed as:

$$\begin{bmatrix} \lambda_\alpha \\ \lambda_\beta \end{bmatrix} = \frac{L_d+L_q}{2} \begin{bmatrix} i_\alpha \\ i_\beta \end{bmatrix} + \frac{L_d-L_q}{2} \begin{bmatrix} cos2\theta_r & sin2\theta_r \\ sin2\theta_r & -cos2\theta_r \end{bmatrix} \begin{bmatrix} i_\alpha \\ i_\beta \end{bmatrix} + \psi_f \begin{bmatrix} cos\theta_r \\ sin\theta_r \end{bmatrix} \tag{A.4}$$

Among them, L_d and L_q are synchronous inductors (H) for the d-axis and q-axis axes; The amplitude of the permanent magnet magnetic flux (Wb) is represented by ψ_{fw};θ_r is the mechanical position angle of the rotor (rad).

Expanding the magnetic flux derivative term in equation (A.1) yields:

DOI: 10.54254/2753-8818/2025.25667

$$\frac{d}{dt}\begin{bmatrix}\lambda_\alpha\\ \lambda_\beta\end{bmatrix}=\frac{d}{dt}\left(\boldsymbol{I}_{s(\alpha\beta)}\begin{bmatrix}i_\alpha\\ i_\beta\end{bmatrix}\right)+\frac{d}{dt}\left(\psi_f\begin{bmatrix}cos\theta_r\\ sin\theta_r\end{bmatrix}\right) \tag{A.5}$$

If the back electromotive force vector e=[e_α, e_β]$_{\wedge T}$ is defined as the induced electromotive force generated by the rotation of the permanent magnet magnetic flux, then:

$$\begin{bmatrix}e_\alpha\\ e_\beta\end{bmatrix}=-\frac{d}{dt}\left(\psi_f\begin{bmatrix}cos\theta_r\\ sin\theta_r\end{bmatrix}\right)=-\psi_f\omega_e\begin{bmatrix}-sin\theta_r\\ cos\theta_r\end{bmatrix} \tag{A.6}$$

Among them, e_α, e_β: the back electromotive force components of the α and β axes (V); ω_e: rotor electrical angular velocity (rad/s), the relationship with mechanical angular velocity ω_r is ω_e=p * ω_r, where p is the number of motor poles; The key factors that make up the back electromotive force are ψ_f and ω_e.

Substitute equations (A.5) and (A.6) into equation (A.1) and reorganize them to represent them in a more general form:

$$\frac{d}{dt}\begin{bmatrix}i_\alpha\\ i_\beta\end{bmatrix}=\boldsymbol{A}\begin{bmatrix}i_\alpha\\ i_\beta\end{bmatrix}+\frac{1}{\boldsymbol{L}_{s(\alpha\beta)}}\left(\begin{bmatrix}v_\alpha\\ v_\beta\end{bmatrix}-\begin{bmatrix}e_\alpha\\ e_\beta\end{bmatrix}-R_s\begin{bmatrix}i_\alpha\\ i_\beta\end{bmatrix}\right)+\boldsymbol{\Delta} \tag{A.7}$$

Appendix B

Define the current estimation error vector:

$$\begin{bmatrix}\tilde{i}_\alpha\\ \tilde{i}_\beta\end{bmatrix}=\begin{bmatrix}i_\alpha-\hat{i}_\alpha\\ i_\beta-\hat{i}_\beta\end{bmatrix} \tag{B.1}$$

Derive the error and substitute the actual system equation (2) and observer equation (3) into:

$$\frac{d}{dt}\begin{bmatrix}\tilde{i}_\alpha\\ \tilde{i}_\beta\end{bmatrix}=\frac{d}{dt}\begin{bmatrix}i_\alpha\\ i_\beta\end{bmatrix}-\frac{d}{dt}\begin{bmatrix}\hat{i}_\alpha\\ \hat{i}_\beta\end{bmatrix}$$

$$=\frac{1}{L_s}\left[-\begin{bmatrix}e_\alpha\\ e_\beta\end{bmatrix}+R_s\begin{bmatrix}\hat{i}_\alpha\\ \hat{i}_\beta\end{bmatrix}-R_s\begin{bmatrix}i_\alpha\\ i_\beta\end{bmatrix}+\begin{bmatrix}\hat{e}_\alpha\\ \hat{e}_\beta\end{bmatrix}+\begin{bmatrix}z_\alpha\\ z_\beta\end{bmatrix}\right]$$

$$=\frac{1}{L_s}\left[-\begin{bmatrix}e_\alpha\\ e_\beta\end{bmatrix}+R_s\begin{bmatrix}-\tilde{i}_\alpha\\ -\tilde{i}_\beta\end{bmatrix}+\begin{bmatrix}\hat{e}_\alpha\\ \hat{e}_\beta\end{bmatrix}+\begin{bmatrix}z_\alpha\\ z_\beta\end{bmatrix}\right]$$

(B.2)

$$=-\frac{R_s}{L_s}\begin{bmatrix}\tilde{i}_\alpha\\ \tilde{i}_\beta\end{bmatrix}+\frac{1}{L_s}\left(\begin{bmatrix}\hat{e}_\alpha-e_\alpha\\ \hat{e}_\beta-e_\beta\end{bmatrix}+\begin{bmatrix}z_\alpha\\ z_\beta\end{bmatrix}\right) \tag{B.3}$$

The sliding mode variable structure control law z is designed as follows:

DOI: 10.54254/2753-8818/2025.25667

$$\begin{bmatrix} z_\alpha \\ z_\beta \end{bmatrix} = k_{smo} \begin{bmatrix} sgn(\tilde{i}_\alpha) \\ sgn(\tilde{i}_\beta) \end{bmatrix} \tag{B.4}$$

To suppress Chattering, Saturation Function is used instead of Sign Function, and Boundary Layer is introduced:

$$z_\alpha = k_{smo} \cdot \text{sat}\left(\frac{\tilde{i}_\alpha}{\Phi}\right), \quad z_\beta = k_{smo} \cdot \text{sat}\left(\frac{\tilde{i}_\beta}{\Phi}\right) \text{sat}\left(x\right) = \begin{cases} sgn(x), & |x| > 1 \\ x, & |x| \le 1 \end{cases} \tag{B.5}$$

Among them, K_{smo}>0: Gain coefficient of sliding mode observer; Φ>0: Boundary layer thickness.

Prove the convergence of the designed SMO using the Lyapunov second method. Construct candidate Lyapunov functions:

$$V = \frac{1}{2} \boldsymbol{s}^T \boldsymbol{s} = \frac{1}{2} \left(\tilde{i}_\alpha^2 + \tilde{i}_\beta^2\right) > 0 \quad \left(\text{for } \mathbf{s} \neq 0\right) \tag{B.6}$$

Derive V:

$$\dot{V} = \boldsymbol{s}^T \dot{\boldsymbol{s}} = \tilde{i}_\alpha \dot{\tilde{i}}_\alpha + \tilde{i}_\beta \dot{\tilde{i}}_\beta \tag{B.7}$$

Substitute into the error dynamic equation (B.3):

$$\dot{V} = \begin{bmatrix} \tilde{i}_\alpha \\ \tilde{i}_\beta \end{bmatrix}^T \left[-\frac{R_s}{L_s} \begin{bmatrix} \tilde{i}_\alpha \\ \tilde{i}_\beta \end{bmatrix} + \frac{1}{L_s} \left(\begin{bmatrix} \Delta e_\alpha \\ \Delta e_\beta \end{bmatrix} + \begin{bmatrix} z_\alpha \\ z_\beta \end{bmatrix} \right) \right] \tag{B.8}$$

Among them, $\Delta e_\alpha = \hat{e}_\alpha - e_\alpha$, $\Delta e\beta = \hat{e}_\beta - e_\beta$ represents the estimation error of back electromotive force. In the initial design phase (with internal ê set to 0), Δe=-e. Consider sliding mode control law (B.5) (z=k_{smo}*sat(ĩ/Φ)), and assume that the back electromotive force is bounded (| e_α |, | e_β | ≤ E_m), parameter resistance R_s>0, inductance L_s>0:

$$\dot{V} = -\frac{R_s}{L_s} \left(\tilde{i}_\alpha^2 + \tilde{i}_\beta^2\right) + \frac{1}{L_s} \left(\Delta e_\alpha \tilde{i}_\alpha + \Delta e_\beta \tilde{i}_\beta + k_{smo} sat\left(\frac{\tilde{i}_\alpha}{\Phi}\right) \tilde{i}_\alpha + k_{smo} sat\left(\frac{\tilde{i}_\beta}{\Phi}\right) \tilde{i}_\beta \right) \tag{B.9}$$

For the case of | $\tilde{i}_\alpha$ |>Φ (sat ($\tilde{i}_\alpha$/Φ)=sgn ($\tilde{i}_\alpha$)):

$$\dot{V} \le -\frac{R_s}{L_s} \left|\tilde{\boldsymbol{i}}\right|^2 + \frac{1}{L_s} \left(\left|\Delta e_\alpha\right| \left|\tilde{i}_\alpha\right| + \left|\Delta e_\beta\right| \left|\tilde{i}_\beta\right| - k_{smo} \left|\tilde{i}_\alpha\right| - k_{smo} \left|\tilde{i}_\beta\right| \right)$$

$$\le -\frac{R_s}{L_s} \left|\tilde{\boldsymbol{i}}\right|^2 + \frac{1}{L_s} \left(2E_m \left|\tilde{\boldsymbol{i}}\right| - k_{smo} \left|\tilde{\boldsymbol{i}}\right| \right) \quad \left(\text{since } \left|\Delta e\right| \le E_m \text{ if } \hat{e} = 0 \right)$$

$$= -\frac{R_s}{L_s} \left|\tilde{\boldsymbol{i}}\right|^2 + \frac{\left|\tilde{\boldsymbol{i}}\right|}{L_s} \left(2E_m - k_{smo}\right)$$

DOI: 10.54254/2753-8818/2025.25667

(B.10)

In order to satisfy $\dot{V}<0$ (ensuring convergence to the boundary layer or sliding surface), the gain k_{smo} needs to be designed to satisfy:

$$k_{smo} > 2E_m \tag{B.11}$$

The maximum possible amplitude of the actual back electromotive force is determined by the motor magnetic flux and the maximum operating speed, where E_m is the maximum possible amplitude of the back electromotive force ($E_m \approx \psi_f * \omega_{\{e,max\}}$).

For the case of $|\tilde{i}_\alpha| \leq \Phi$, $|\tilde{i}_\beta| \leq \Phi$ (sat $(\tilde{i}_\alpha/\Phi) = \tilde{i}_\alpha/\Phi$), the analysis is relatively complex, and it is generally believed that the system can work stably in the boundary layer.

By selecting a sufficiently large sliding mode gain $k_{smo} > 2E_m$, it can be ensured that $\dot{V}<0$ holds outside the boundary layer, that is, the observation errors $\tilde{i}_\alpha$ and $\tilde{i}_\beta$ will converge to the interior or vicinity of the boundary layer $|\tilde{i}| \leq \Phi$ within a finite time, thereby ensuring the effectiveness of the back electromotive force estimation.

DOI: 10.54254/2753-8818/2025.25667

Appendix C

Table 1. Key parameters table

Category	Specific Item	Parameter/Specification/Model
PMSM	Motor Model	750W, 4-pole IPMSM
	Rated Power	750 W
	Rated Speed	3000 rpm
	Rated Torque	2.39 Nm
	Stator Resistance (Rs)	1.8 Ω
	Direct-axis Inductance (Ld)	8.5 mH
	Quadrature-axis Inductance (Lq)	12.0 mH
	Permanent Magnet Flux Linkage (ψ_f)	0.15 Wb
	Number of Pole Pairs (P)	2
Simulation Platform	Software Environment	MATLAB/Simulink R2023b, PLECS Blockset 4.6
	Simulation Step Size	5 μs
Experimental Platform	Controller Hardware	Texas Instruments TMS320F28379D Dual-Core Delfino DSC
	Power Driver	Three-phase Full-bridge IGBT Inverter (1200V, 25A)
	Voltage/Current Sensors	LEM LV 25-P (Voltage), LEM LA 55-P
	Position/Speed Reference Sensor	2500-line Incremental Optical Encoder
	Load Device	Magnetic Powder Brake + Torque Sensor
	DC Power Supply	300V DC Regulated Power Supply
Control Algorithm Parameters	PWM Switching Frequency	10 kHz
	Current Sampling Frequency	10 kHz (Synchronized PWM Midpoint Sampling)
	Speed Control Frequency	1 kHz
SMO Parameters	Sliding Mode Gain (k_{smo})	20
	Boundary Layer Thickness (Φ)	0.5 A
	Back-EMF LPF Cutoff Frequency	500 Hz
PLL Parameters	P Gain (Kp_pll)	150 rad/(s·rad)
	I Gain (Ki_pll)	5000 rad/(s²·rad)
SMC Parameters	Sliding Surface Coefficient (λ)	50 rad/s
	Switching Gain (K_sw)	15 A/(rad/s)
	Boundary Layer Thickness (Φ_ω)	10 rpm
Baseline Controller Parameters	PI Speed Controller Parameters (KP, KI)	KP = 0.05 A/(rad/s), KI = 0.5 A/(rad·s)
	PI Current Controller Parameters (αβ-axis)	KP = 1.0 Ω, KI = 3000 rad/s
Subsequent Test Conditions	Speed Range	Low Speed: 100 rpm, Medium Speed: 1500 rpm, High Speed: 3000 rpm
	Speed Step	500 rpm → 1500 rpm (Rated)
	Load Step	No Load → 100% Rated Torque
	Parameter Robustness Test	Rs Variation: +50%, L_d/L_q Variation: +30%, -30%, ψ_f Variation: ±15%, ±10%

DOI: 10.54254/2753-8818/2025.25667

Appendix D

Table 2. Experimental results of parameter robustness analysis

Parameter Perturbation	Operating Condition	Position Error RMS (deg)	Error Increase	Speed Steady-State Error (rpm)	Error Increase	Current THD (%)	Key Conclusion
Nominal Parameters	200rpm + 0% Load	1.50	–	0.5	–	4.5	Baseline
(Rs=1.8Ω, Ld =8.5mH,	3000rpm + 100% Load	0.55	–	5.0	–	5.8	
Lq=12mH, ψf =0.15Wb)	1500rpm + Load Step*	0.80	–	–	–	–	
Rs +50%	200rpm + 0% Load	1.58	+5.3%	0.6	+20%	5.1	Minor impact
(→2.7Ω)	3000rpm + 100% Load	0.57	+3.6%	5.3	+6%	6.2	
Ld –30%	200rpm + 0% Load	1.95	+30.0%	0.7	+40%	4.7	Transient degradation
(→5.95mH)	3000rpm + 100% Load	0.70	+27.3%	5.9	+18%	6.0	
Lq +30%	200rpm + 0% Load	1.80	+20.0%	0.6	+20%	4.6	Increased position jitter
(→15.6mH)	3000rpm + 100% Load	0.65	+18.2%	5.7	+14%	5.9	
ψf –10%	200rpm + 0% Load	1.55	+3.3%	2.0	+300%	4.6	Speed accuracy bottleneck
(→0.135Wb)	3000rpm + 100% Load	0.58	+5.5%	15.0	+200%	5.9	
	1500rpm + Load Step*	0.85	+6.3%	12.0	+140%	–	
ψf –15%	200rpm + 0% Load	1.60	+6.7%	3.5	+600%	4.7	Critical speed drift
(→0.1275Wb)	3000rpm + 100% Load	0.60	+9.1%	24.0	+380%	6.1	
	1500rpm + Load Step*	0.88	+10.0%	18.0	+170%	–	
ψf +10%	200rpm + 0% Load	1.52	+1.3%	-1.8	-460%	4.4	Overcompensation
(→0.165Wb)	3000rpm + 100% Load	0.56	+1.8%	-8.0	-260%	5.7	